Catalysis Today 180 (2012) 111–116

Contents lists available at ScienceDirect

Catalysis Today

journal homepage: www.elsevier.com/locate/cattod

Syngas production by partial oxidation of methane over $Pt/CeZrO_2/Al_2O_3$ catalysts

Fabiano A. Silva[a], Karen A. Resende[a], Adriana M. da Silva[b], Kátia R. de Souza[b], Lisiane V. Mattos[c], Mario Montes[d], Eduardo F. Souza-Aguiar[e], Fabio B. Noronha[b], Carla E. Hori[a,*]

[a] Faculdade de Engenharia Química – Universidade Federal de Uberlândia, Av. João Naves de Ávila, 2160, bloco 1K, Campus Santa Mônica, CEP 38408-144, Uberlândia – MG, Brazil
[b] Instituto Nacional de Tecnologia – INT, Av. Venezuela, 82, Centro, CEP 20081-312, Rio de Janeiro – RJ, Brazil
[c] Universidade Federal Fluminense, Rua Passo da Pátria, 156, Niterói, RJ CEP 24210-240 – Brazil
[d] Department of Applied Chemistry, University of the Basque Country (UPV-EHU), Apdo. 1072, 20080 San Sebastián, Spain
[e] Petrobras Research Centre (CENPES), Ilha do Fundão, Q7, Cidade Universitária, CEP 21949-900, Rio de Janeiro, Brazil

ARTICLE INFO

Article history:
Received 20 December 2010
Received in revised form 4 May 2011
Accepted 9 July 2011
Available online 27 August 2011

Keywords:
Partial oxidation of methane
$Pt/CeZrO_2/Al_2O_3$ catalysts
Syngas
Hydrogen production

ABSTRACT

In this study, we evaluated the effect of ceria–zirconia content on the performance of $Pt/x\%CeZrO_2/Al_2O_3$ (x = 0–40 wt.%) during partial oxidation of methane. X-ray diffraction results indicated that, for samples containing 10 and 20 wt.% of $CeZrO_2$, there was the formation of a homogeneous solid solution between ceria and zirconia. On the other hand, for $Pt/30\%CeZrO_2/Al_2O_3$, there was the formation of a ceria rich phase and a zirconia rich phase whereas a ceria rich phase and an isolated zirconia phase were detected for $Pt/40\%CeZrO_2/Al_2O_3$. Catalytic tests showed that Pt/Al_2O_3 exhibited a significant deactivation, while $Pt/10\%CeZrO_2/Al_2O_3$ and $Pt/20\%CeZrO_2/Al_2O_3$ practically did not loose their activity after 24 h. A deactivation was detected for $Pt/30\%CeZrO_2/Al_2O_3$ and $Pt/40\%CeZrO_2/Al_2O_3$. The higher stability of the $Pt/10\%CeZrO_2/Al_2O_3$ and $Pt/20\%CeZrO_2/Al_2O_3$ catalysts was attributed to the high reducibility and consequently the high oxygen mobility of the homogeneous solid solution formed, which promoted the mechanism of carbon removal from the metallic particle.

1. Introduction

Over the past two decades, a lot of attention has been given to the study of the production of H_2 and syngas through the partial oxidation of methane (POM) [1]. The renewed interest on POM was stimulated by the increasing demand of H_2 and other cleaner fuels, as well as, some advantages that POM presents. For instance, POM is a mildly exothermic reaction, unlike steam and dry reforming of methane and therefore, it is a more energy efficient process. At temperatures above 1000 K, the reaction can lead to 100% methane conversions with high selectivities to hydrogen and CO formation. In addition, for process integration, POM provides a H_2/CO ratio of 2, which is the ratio ideal for Fischer–Tropsch synthesis and methanol synthesis [2].

One of the main problems that have to be overcome in order to produce H_2 and syngas from POM commercially is the stability of the catalyst. Usually, the formation of carbon deposits on the catalysts surface leads to the deactivation and low H_2 selectivity. In order to inhibit carbon deposition, the use of a noble metal, such as Pt, has been investigated with a great deal of interest [3–5]. In particular, zirconia and ceria–zirconia supported Pt catalysts have shown high activity and stability for the POM reaction [5–11]. The improved performance was attributed to the higher reducibility and oxygen storage/release capacity of $Pt/CeZrO_2$ catalysts, which promotes the mechanism of carbon removal from the active sites, favoring the stability of the catalysts. Metal dispersion also plays an important role on the performance of catalyst for POM [4]. $Pt/Ce_xZr_{1-x}O_2$ catalysts presented higher stability than Pt/CeO_2 and Pt/ZrO_2 catalysts. These results were attributed to a proper balance between oxygen transfer ability of the support and metal dispersion. However, when calcined at high temperatures, ceria–zirconia supports exhibit very low surface area, which provides poor metal dispersion. To improve metal dispersion, ceria–zirconia may be deposited over a high surface area oxide such as alumina. The preparation method and the Ce/Zr ratio significantly affected the redox properties of these materials and consequently their catalytic performances. We have studied the effect of the preparation method and the Ce/Zr ratio on the performance of $Pt/Ce_xZr_{1-x}O_2/Al_2O_3$ catalysts for the POM [9–11]. These studies showed that impregnation of ceria or ceria–zirconia on alumina provided a higher coverage degree of alumina than precipitation technique. This resulted on higher metal and ceria interaction for these samples, which was responsible for the higher stability and better CO and H_2 selectivities on the methane partial oxidation observed for these catalysts [9]. The Ce/Zr ratio significantly affects the oxygen storage capacity, which is fundamental for

* Corresponding author. Tel.: +55 34 3239 4292; fax: +55 34 3239 4249.
E-mail address: cehori@ufu.br (C.E. Hori).

0920-5861/$ – see front matter © 2011 Elsevier B.V. All rights reserved.
doi:10.1016/j.cattod.2011.07.035

keeping the metal surface free of carbon deposits and thus catalyst stability. We have reported that $Pt/Ce_{0.50}Zr_{0.50}O_2/Al_2O_3$ exhibited the highest activity and stability due to the appropriated balance between the high oxygen storage capacity and degree of alumina coverage [10].

However, to our knowledge, the literature still does not report the effect of the $CeZrO_2$ content on the properties of $Pt/CeZrO_2/Al_2O_3$ catalysts. Therefore, in this work we decide to examine the use of different ceria–zirconia loadings (0–40 wt.%) on $Pt/CeZrO_2/Al_2O_3$ and to evaluate the effect on the physical and chemical properties and on the catalytic performance during POM.

2. Experimental

2.1. Catalysts preparation

Alumina supports were prepared by calcination of bohemite (Catapal-A – Sasol) at 1173 K for 6 h in a muffle. The alumina supported ceria–zirconia samples were prepared by co-impregnation of the alumina with an aqueous solution of cerium (IV) ammonium nitrate (Aldrich) and zirconium nitrate (MEL Chemicals) as precursors of cerium and of zirconium, respectively. For each sample, the aqueous solution was prepared to obtain $CeZrO_2$ loadings of 10, 20, 30 and 40 wt.% and a Ce/Zr ratio of 1 in one impregnation procedure. The samples were dried at 373 K for 12 h and then calcined in a muffle furnace at 1073 K for 4 h. Then, the catalysts were prepared by incipient wetness impregnation of the supports with an aqueous solution of H_2PtCl_6 (Aldrich) in order to obtain 1.5 wt.% of Pt. The samples were dried at 393 K for 12 h and calcined under air (50 mL/min) at 673 K for 2 h.

2.2. Textural characterization

The texture of all samples was characterized by nitrogen adsorption, using a Quantasorb Jr. (Quantachrome) equipment endowed with a thermal conductivity detector. This equipment uses the dynamic method and each experiment was performed with 5 different nitrogen concentrations. The catalyst was dried under N_2 flow at 423 K for 16 h. The adsorption isotherms were determined by nitrogen adsorption at 77 K.

2.3. X-ray fluorescence (XRF)

The cerium, platinum, and zirconium contents of each catalyst were determined on a Rigaku RIX 3100 X-ray spectrometer with a rhodium tube operated at 4 KW. The measurement technique applied was a semi-quantitative analysis. Calcined samples (~0.5 g) were analyzed as self-supported wafers.

2.4. X-ray diffraction (XRD)

The catalysts were analyzed by powder X-ray diffraction (Philips PW3710), using Cu Kα radiation (λ = 1.5406 Å). XRD patterns were collected through two different procedures: (i) in the range of 2θ from 25 to 90°, at a scan speed of 0.04°/step and counting times of 1 s/step and (ii) 2θ from 27 to 32°, at a scan speed of 0.02°/step and counting times of 10 s/step.

2.5. Temperature programmed reduction (TPR)

TPR measurements were carried out in a multipurpose unit connected to a quadrupole mass spectrometer (Balzers, Omnistar). The samples (300 mg) were dehydrated at 423 K for 30 min in a He flow prior to reduction. After cooling to room temperature under He, a mixture of 2% H_2 in Ar flowed through the sample at 30 mL/min, raising the temperature at a heating rate of 10 K/min up to 1273 K. The hydrogen consumption was monitored by the quadrupole mass spectrometer. In order to determine the H_2 consumption, a calibrated volume of pure H_2 was injected into the mass spectrometer at the end of each experiment. This procedure was performed at least 3 times and an average was obtained.

2.6. Metal dispersion

The dehydrogenation of cyclohexane was used as an insensitive structure reaction in order to determine the apparent metallic dispersion of ceria–zirconia supported Pt catalysts. In this case, more traditional techniques such as H_2 or CO chemisorption are not recommended for these catalysts due to the possibility of adsorption of both gases on ceria [5,12]. The dispersions of different Pt/Al_2O_3 samples were determined by H_2 chemisorption and the rate of cyclohexane dehydrogenation was also measured for each one. Such correlation was used successfully before to estimate the catalyst dispersion values [8,10].

The reaction was performed at 10^5 Pa in a flow micro-reactor. The sample (10 mg) was previously dried in situ under N_2 flow (30 mL/min) at 393 K during 30 min. Then, the sample was cooled to room temperature and heated under pure hydrogen flow to 733 K at a heating rate of 10 K/min. This temperature was held for 1 h. The sample was cooled in hydrogen flow to 543 K. The reaction mixture was obtained by bubbling hydrogen through a saturator containing cyclohexane (99.9%) at 285 K (H_2/C_6H_{12} = 13.2). The space velocity was (WHSV) 170 h^{-1} and the reaction temperatures varied from 520 to 570 K. At these conditions, no mass transfer or equilibrium limitations were observed. The conversions were kept below 10%. The composition of effluent gas phase was measured by online gas chromatograph (Shimatzu GC 17-A) equipped with a thermal conductivity detector and a Chrompack CP-WAX 57 CB column.

2.7. Catalytic test

Partial oxidation (POX) of methane was performed in a quartz reactor at atmospheric pressure. Catalyst samples (20 mg) were diluted with SiC (SiC/catalyst ratio = 3.0). Prior to the reaction, the catalyst was reduced under H_2 at 773 K for 1 h and then heated to 1073 K under N_2. The reactions were carried out at 1073 K over all catalysts. POX was performed with a reactant mixture containing a CH_4:O_2 ratio of 2:1 and a flow rate of 100 mL/min. The exit gases were analyzed using a gas chromatograph (Agilent 6890) equipped with a thermal conductivity detector and a Carboxen 1010 column (Supelco).

3. Results and discussion

3.1. Catalyst characterization

3.1.1. BET surface area and chemical composition

Table 1 presents the values of BET surface areas and chemical composition obtained for all catalysts. Increasing ceria–zirconia content continuously decreased the BET surface area. All the sam-

Table 1
BET surface area and chemical composition obtained by X-ray fluorescence.

Samples	BET surface area (m^2/g)	Composition (wt.%)				
		Pt	CeO_2	ZrO_2	Al_2O_3	Cl
Pt/Al_2O_3	114	1.5	0.0	0.0	96.8	1.5
$Pt/10\%CeZrO_2/Al_2O_3$	99	1.6	5.4	4.6	86.9	1.3
$Pt/20\%CeZrO_2/Al_2O_3$	90	1.7	12.2	9.9	74.7	1.2
$Pt/30\%CeZrO_2/Al_2O_3$	79	1.5	16.6	12.3	68.2	1.1
$Pt/40\%CeZrO_2/Al_2O_3$	72	1.6	23.8	19.4	53.9	1.1

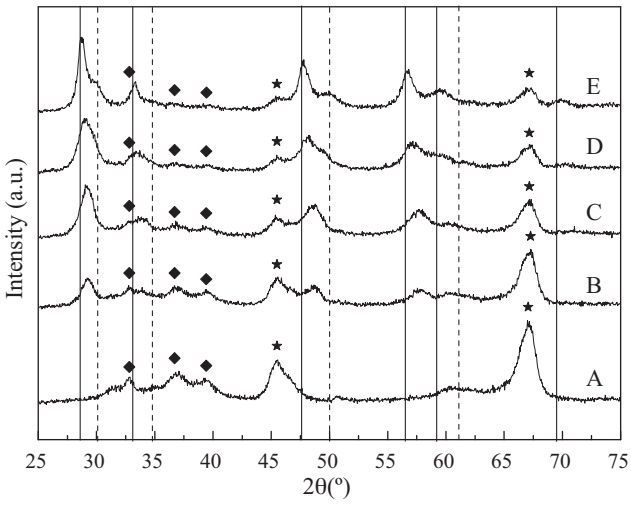

Fig. 1. X-ray diffraction patterns obtained between 25 and 75° for: (a) Pt/Al_2O_3; (b) $Pt/10\%CeZrO_2/Al_2O_3$; (c) $Pt/20\%CeZrO_2/Al_2O_3$; (d) $Pt/30\%CeZrO_2/Al_2O_3$; (e), $Pt/40\%CeZrO_2/Al_2O_3$. The symbols (⋆) and (♦) are the characteristics lines of γ-alumina and θ-alumina, respectively. The solid vertical lines are characteristic of the cubic ceria structure and the broken vertical lines correspond to the tetragonal zirconia phase.

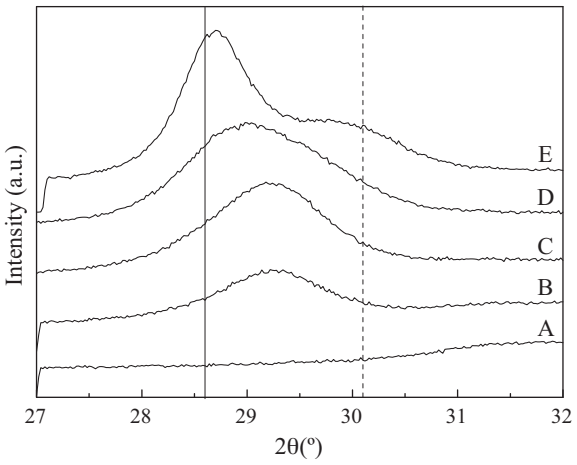

Fig. 2. X-ray diffraction patterns obtained between 2θ = 27 and 32° for (a) Pt/Al_2O_3; (b) $Pt/10\%CeZrO_2/Al_2O_3$; (c) $Pt/20\%CeZrO_2/Al_2O_3$; (d) $Pt/30\%CeZrO_2/Al_2O_3$; (e) $Pt/40\%CeZrO_2/Al_2O_3$. The solid vertical lines are characteristic of the cubic ceria peaks and the broken vertical lines correspond to the tetragonal zirconia phase.

ples presented chemical composition close to the nominal values. We also could detect the presence of chloride, which is somewhat common when using H_2PtCl_6 as a Pt precursor, despite the calcination in air flow.

3.1.2. Effect of ceria–zirconia content on the formation of a solid solution

XRD patterns of Pt/Al_2O_3 and $Pt/x\%CeZrO_2/Al_2O_3$ are presented in Fig. 1. The XRD pattern of Pt/Al_2O_3 catalyst (curve A) exhibited the lines characteristics of γ and θ-alumina phases. In the case of $Pt/x\%CeZrO_2/Al_2O_3$ samples containing different $CeZrO_2$ loadings, in addition to the lines characteristic of γ and θ-alumina phases, the diffratograms (curves B–E) also revealed the presence of the lines corresponding to cerium oxide with cubic structure. However, all the lines related to the ceria phase were shifted to higher 2θ positions. For example, the diffraction lines of Ce (1 1 1) were shifted from $2\theta = 28.6°$ (CeO_2, JCPDS-4-0593) to 29.2°, 29.04°, 28.96° and 28.68° for $Pt/10\%CeZrO_2/Al_2O_3$, $Pt/20\%CeZrO_2/Al_2O_3$, $Pt/30\%CeZrO_2/Al_2O_3$ and $Pt/40\%CeZrO_2/Al_2O_3$ catalysts, respectively. This shift indicates the formation of a solid solution between the cerium and zirconium oxides [13–16]. It is important to stress that increasing the ceria–zirconia content decreased the extent of this shift, which was no longer observed for the sample containing 40 wt.% $CeZrO_2$. Furthermore, it is clearly observed the appearance of a shoulder on the diffraction lines of $Pt/30\%CeZrO_2/Al_2O_3$ and $Pt/40\%CeZrO_2/Al_2O_3$ samples. In order to evaluate in greater detail the position and the shape of Ce (1 1 1) reflection, data collection with a slow scanning speed was performed for $Pt/CeZrO_2/Al_2O_3$ samples and the results were presented in Fig. 2. The XRD pattern showed that the peak at $2\theta = 29.4°$ is symmetrical only for the samples containing 10 and 20 wt.% $CeZrO_2$, indicating the formation of a homogeneous solid solution with the expected composition ($Ce_{0.50}Zr_{0.50}O_2$). For the $Pt/30\%CeZrO_2/Al_2O_3$ sample, the shoulder at around $2\theta = 29.5°$ suggested that not all the zirconium was incorporated into the ceria lattice, leading to the formation of a solid solution with different composition. In fact, the diffratogram of $Pt/40\%CeZrO_2/Al_2O_3$ sample revealed the presence of a shoulder at 30.1°, indicating the segregation of an isolated zirconia phase.

There are several studies in the literature reporting the effect of preparation method and Ce/Zr ratio on the formation of a ceria–zirconia solid solution. Kozlov et al. [13] studied ceria–zirconia supported on alumina samples (Ce/Zr ratio of 1) prepared by co-impregnation and sol–gel method. For the samples prepared by impregnation, a ceria rich mixed oxide ($Ce_{0.7}Zr_{0.3}O_2$) and a zirconia rich phase were formed instead of the expected nominal composition ($Ce_{0.50}Zr_{0.50}O_2$). Silva et al. [9] reported the formation of $Ce_{0.82}Zr_{0.18}O_2$ solid solution for $Pt/Ce_{0.75}Zr_{0.25}O_2/Al_2O_3$ samples prepared by impregnation and precipitation, whereas a zirconia rich phase was not detected. Silva et al. [10] also investigated the effect of the Ce/Zr ratio on $Pt/Ce_xZr_{1-x}O_2/Al_2O_3$ catalysts prepared by impregnation. Depending on the Ce/Zr ratio, a ceria–zirconia solid solution with different composition was formed. For the $Pt/Ce_{0.50}Zr_{0.50}O_2/Al_2O_3$ catalyst, there was the formation of a ceria–zirconia solid solution with a composition of $Ce_{0.61}Zr_{0.39}O_2$ and an isolated zirconia phase.

However, we could not find studies in the literature about the effect of ceria–zirconia content on the formation of a solid solution. Based on the methodology proposed by Kozlov et al. [13], we estimated the real composition of our supported ceria–zirconia samples (the nominal Ce/Zr ratio for all different $CeZrO_2$ loadings was 1, or a $Ce_{0.5}Zr_{0.5}O_2$ mixed oxide). $Pt/10\%CeZrO_2/Al_2O_3$ and $Pt/20\%CeZrO_2/Al_2O_3$ samples exhibited solid solutions with compositions close to the expected nominal one ($Ce_{0.45}Zr_{0.55}O_2$ and $Ce_{0.54}Zr_{0.46}O_2$, respectively). On the other hand, a $Ce_{0.67}Zr_{0.33}O_2$ solid solution was formed for the sample containing 30wt.%$CeZrO_2$, while there was the formation of a ceria–zirconia solid solution with a composition of $Ce_{0.85}Zr_{0.15}O_2$ and an isolated zirconia phase for $Pt/40\%CeZrO_2/Al_2O_3$ sample.

Therefore, in our work, the results revealed that low $CeZrO_2$ loading favored the incorporation of zirconium into the ceria lattice, leading to the formation of a homogeneous solid solution. Above 30 wt.% of $CeZrO_2$, the segregation of an isolated zirconia phase occurred.

3.1.3. Catalysts reducibility

TPR profiles of Pt/Al_2O_3, $Pt/10\%CeZrO_2/Al_2O_3$, $Pt/20\%CeZrO_2/Al_2O_3$, $Pt/30\%CeZrO_2/Al_2O_3$ and $Pt/40\%CeZrO_2/Al_2O_3$ catalysts are presented in Fig. 3. For Pt/Al_2O_3 sample (profile A), only a low temperature reduction peak at 509 K is observed. Usually this reduction peak is attributed to the reduction of $PtCl_xO_y$ (oxychloride platinum) species on the alumina surface [17].

$Pt/10\%CeZrO_2/Al_2O_3$ and $Pt/20\%CeZrO_2/Al_2O_3$ catalysts (profiles B and C) exhibited a single hydrogen consumption peak

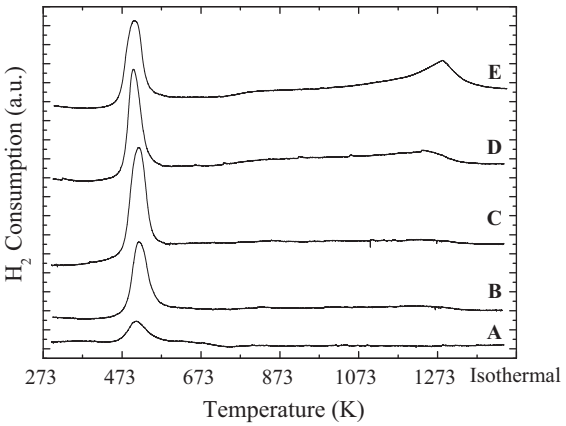

Fig. 3. Temperature programmed reduction profiles for (a) Pt/Al_2O_3; (b) $Pt/10\%CeZrO_2/Al_2O_3$; (c) $Pt/20\%CeZrO_2/Al_2O_3$; (d) $Pt/30\%CeZrO_2/Al_2O_3$; (e) $Pt/40\%CeZrO_2/Al_2O_3$.

at low temperature region around 515 K. This peak is generally attributed to the reduction of platinum oxide and to the promoted reduction of surface ceria by metallic platinum formed [4,8]. For $Pt/30\%CeZrO_2/Al_2O_3$ and $Pt/40\%CeZrO_2/Al_2O_3$ samples (profiles D and E, respectively), besides the H_2 consumption at low temperatures, around 505 K for both samples, there is also a high temperature peak at 1246 K in profile D and at 1273 K in profile E. These high temperature peaks can be attributed to the reduction of CeO_2 in the bulk phase [18]. The comparison between TPR profiles of $Pt/x\%CeZrO_2/Al_2O_3$ catalysts reveals that only the catalysts containing a high $CeZrO_2$ content exhibits a H_2 uptake at high temperature region. According to XRD results, only a small amount of zirconium entered in the cerium oxide lattice in these samples. In fact, the addition of zirconium oxide to ceria structure favors the redox properties, increasing the number of oxygen vacancies. Consequently, this higher oxygen mobility increases the cerium–zirconium mixed oxide reducibility, which explains the absence of hydrogen consumption at high temperature for the $Pt/10\%CeZrO_2/Al_2O_3$ and $Pt/20\%CeZrO_2/Al_2O_3$ samples [13,14,16]. Hydrogen consumption uptakes for catalysts are presented in Table 2. As the $CeZrO_2$ content increases, the H_2 consumption during TPR also increased, as one could expect.

3.1.4. Metal dispersion

The reaction rates of dehydrogenation of cyclohexane for all catalysts, as well as the apparent metallic dispersion are presented in Table 2. The samples presented similar Pt dispersions around 65%, which are in agreement with previous results reported by our group for this kind of catalysts [11].

Table 2
H_2 consumptions during TPR and apparent metal dispersions calculated by dehydrogenation of cyclohexane.

Sample	TPR H_2 uptake ($\mu mol/g_{cat}$)	Cyclohexane dehydrogenation	
		Rate ($mol/g_{cat}\,h$)	Pt dispersion (%)[a]
Pt/Al_2O_3	77	0.2482	65
$Pt/10\%CeZrO_2/Al_2O_3$	291	0.2479	58
$Pt/20\%CeZrO_2/Al_2O_3$	483	0.3115	64
$Pt/30\%CeZrO_2/Al_2O_3$	588	0.2248	57
$Pt/40\%CeZrO_2/Al_2O_3$	783	0.2932	68

[a] Values calculated using the real Pt content measured by XRF.

3.2. Partial oxidation of methane

Fig. 4 shows the methane conversion and products selectivity versus time on stream (TOS) for all catalysts on partial oxidation of methane. The initial methane conversions were similar (65 -70%) for all samples studied. This result is in agreement with the values of metallic dispersion obtained, which were similar for all samples (Table 2).

Pt/Al_2O_3 catalyst exhibited a significant deactivation during the reaction, while $Pt/10\%CeZrO_2/Al_2O_3$ and $Pt/20\%CeZrO_2/Al_2O_3$ catalysts practically did not loose their activity after 24 h TOS. Furthermore, a slight deactivation was detected over $Pt/30\%CeZrO_2/Al_2O_3$ and $Pt/40\%CeZrO_2/Al_2O_3$. The addition of $CeZrO_2$ to Pt/Al_2O_3 catalyst improved the stability of the samples. However, this effect is more significant for $CeZrO_2$ content lower than 30%.

Silva et al. [10] reported similar results for $Pt/14\%Ce_{0.5}Zr_{0.5}O_2/Al_2O_3$ and Pt/Al_2O_3 catalysts during partial oxidation of methane. They observed that $Pt/14\%Ce_{0.5}Zr_{0.5}O_2/Al_2O_3$ was quite stable, whereas methane conversion significantly decreased on Pt/Al_2O_3 during the reaction. The better catalytic performance of $Pt/14\%Ce_{0.5}Zr_{0.5}O_2/Al_2O_3$ was explained by the appropriate balance between a good degree of alumina coverage and excellent oxygen storage capacities of this sample. These characteristics promoted the cleaning mechanism, maintaining the surface free of carbon deposits.

Regarding selectivity to the products, it was detected the formation of H_2, CO, CO_2 and H_2O for all catalysts. The H_2 selectivity followed the same trend as methane conversion (Fig. 4). The production of H_2 significantly decreased during the reaction for Pt/Al_2O_3 catalyst, whereas it remained unchanged for $Pt/10\%CeZrO_2/Al_2O_3$ and $Pt/20\%CeZrO_2/Al_2O_3$ catalysts. For $Pt/30\%CeZrO_2/Al_2O_3$ and $Pt/40\%CeZrO_2/Al_2O_3$ catalysts, the H_2 selectivity slightly decreased during 24 h TOS.

In the case of CO and CO_2 selectivities (Fig. 4), no important changes were observed during the reaction for $Pt/10\%CeZrO_2/Al_2O_3$ and $Pt/20\%CeZrO_2/Al_2O_3$ catalysts. However, a significant variation of the selectivity to CO and CO_2 was observed for the other catalysts. The production of CO_2 increased and the selectivity to CO decreased as the methane conversion decreased. Thus the deactivation of these catalysts was followed by the increase of CO_2 selectivity. This effect is much more significant for Pt/Al_2O_3 catalyst.

These results are likely explained through a two-step mechanism that has been proposed for the partial oxidation of methane [19–21]. According to this mechanism, in the first stage, CO_2 and H_2O were produced by methane combustion. In the second step, synthesis gas is formed via carbon dioxide and steam reforming reaction of the unreacted methane.

Recently, we have studied the partial oxidation of methane over Pt/Al_2O_3 and $Pt/CeZrO_2$ using Temperature-Programmed Surface Reaction (TPSR) experiments [4,22]. The TPSR results are in agreement with this two step mechanism of the partial oxidation of methane, involving the combustion of methane followed by CO_2 and H_2O methane reforming.

Therefore, the increase of CO_2 production on Pt/Al_2O_3, $Pt/30\%CeZrO_2/Al_2O_3$ and $Pt/40\%CeZrO_2/Al_2O_3$ catalysts suggest that the CO_2 methane reforming was inhibited during the reaction over these samples. The inhibition of CO_2 reforming is likely attributed to the increase of carbon deposits around or near the metal particle that affects the CO_2 dissociation on the support.

In the case of $Pt/10\%CeZrO_2/Al_2O_3$ and $Pt/20\%CeZrO_2/Al_2O_3$ catalysts, the selectivity to CO practically did not change during the reaction due to the formation of a homogeneous solid solution that

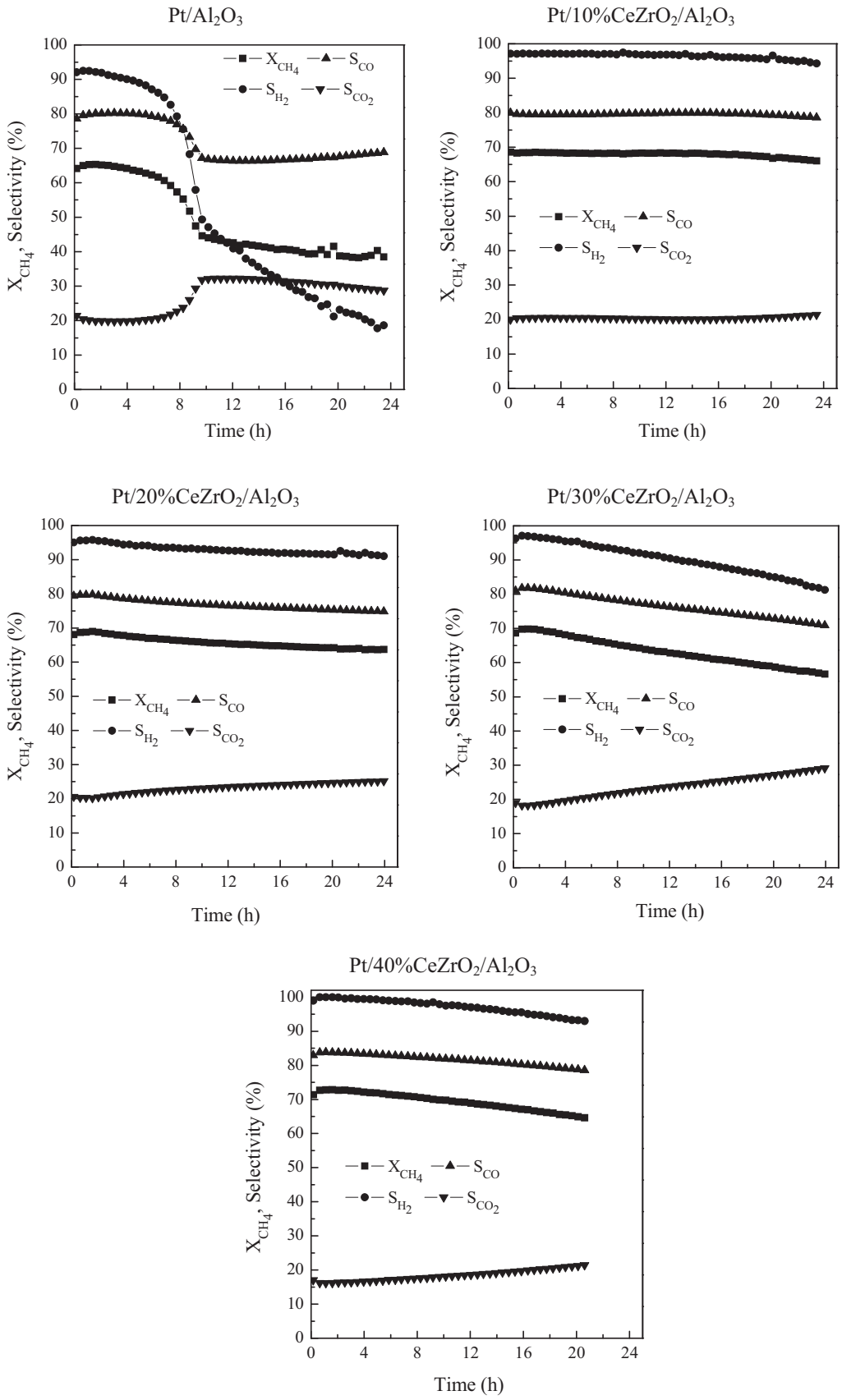

Fig. 4. Methane conversion and product selectivities versus time on stream for partial oxidation of methane over (A) Pt/Al_2O_3; (B) $Pt/10\%CeZrO_2/Al_2O_3$; (C) $Pt/20\%CeZrO_2/Al_2O_3$; (D) $Pt/30\%CeZrO_2/Al_2O_3$; (E) $Pt/40\%CeZrO_2/Al_2O_3$.

exhibits higher oxygen mobility and promotes the mechanism of carbon removal.

4. Conclusions

In this study, we investigated the effect of different $CeZrO_2$ loadings on the catalytic properties and performance for POM reaction over Pt/*x*%$CeZrO_2/Al_2O_3$ catalysts (*x* = 0–40 wt.%). The characterization results showed that both BET surface areas and metallic dispersions did not varied significantly with the increase of the ceria–zirconia mixed oxide content. However, XRD results indicate that, for samples containing 10 and 20 wt.% of $CeZrO_2$, there was the formation of a homogeneous solid solution. On the other hand, for catalysts containing higher ceria–zirconia loadings (30 and 40 wt.%), the solid solution formed was not homogeneous, with evidence of an isolated zirconia phase. During catalytic tests, initially all the samples presented similar activities. Over the reaction period, Pt/Al_2O_3 and the samples containing 30 and 40 wt.% of $CeZrO_2$ deactivated, with H_2 and CO selectivities dropping and CO_2 formation increasing. On the other hand, the samples with a homogeneous ceria–zirconia solid solution (Pt/10%$CeZrO_2/Al_2O_3$ and Pt/20%$CeZrO_2/Al_2O_3$) remained quite stable during TOS, which is likely due to high oxygen mobility in the lattice, which helped to keep the surface of the catalysts free of carbon deposits.

Acknowledgements

F.A. Silva wishes to acknowledge the scholarship received from CAPES and CNPq.

References

[1] B.C. Enger, R. Lodeng, A. Holmen, Appl. Catal. A: Gen. 346 (2008) 1–27.
[2] R. Horn, K.A. Williams, N.J. Degenstein, L.D. Schmidt, J. Catal. 242 (2006) 92–102.
[3] C.H. Au,.C.F. Ng, M.S. Liau, J. Catal. 185 (1999) 12–22.
[4] L.V. Mattos, E.R. de Oliveira, P.D. Resende, F.B. Noronha, F.B. Passos, Catal. Today 77 (2002) 245.
[5] P. Pantu, G. Gavalas, Appl. Catal. A: Gen. 223 (2002) 253–260.
[6] M.E.S. Hegarty, A.M. O'Connor, J.R.H. Ross, Catal. Today 42 (1998) 225.
[7] A.M. O'Connor, J.R.H. Ross, Catal. Today 46 (1998) 203.
[8] F.B. Passos, E.R. de Oliveira, L.V. Mattos, F.B. Noronha, Catal. Today 101 (2005) 23.
[9] P.P. Silva, F.A. Silva, H.P. Souza, A.G. Lobo, L.V. Mattos, F.B. Noronha, C.E. Hori, Catal. Today 101 (2005) 31.
[10] P.P. Silva, F.A. Silva, L.S. Portela, L.V. Mattos, F.B. Noronha, C.E. Hori, Catal. Today 107 (2005) 734.
[11] F.A. Silva, J.A.C. Ruiz, K.R. Souza, J.M.C. Bueno, L.V. Mattos, F.B. Noronha, C.E. Hori, Appl. Catal. A: Gen. 364 (2009) 122–129.
[12] E. Rogemond, N. Essayem, R. Frety, V. Perrichon, M. Primet, F. Mathis, J. Catal. 166 (1997) 229.
[13] A.I. Kozlov, D.H. Kim, A. Yezerets, P. Andersen, H.H. Kung, M.C. Kung, J. Catal. 209 (2002) 417.
[14] C.E. Hori, H. Permana, K.Y. Simon Ng, A. Brenner, K. More, K.M. Rahmoeller, D. Belton, Appl. Catal. B: Environ. 16 (1998) 105.
[15] T. Murota, T. Hasegawa, S. Aozasa, H. Matsui, M. Motoyama, J. Alloys Compd. 193 (1993) 298.
[16] A. Trovarelli, F. Zamar, J. Llorca, C. de Leitenburg, G. Dolcetti, J.T. Kiss, J. Catal. 169 (1997) 490.
[17] S. Damyanova, J.M.C. Bueno, Appl. Catal. A: Gen. 253 (2003) 135.
[18] H.C. Yao, Y.F.Y. Yao, J. Catal. 86 (1984) 254.
[19] D. Dissanayake, M.P. Rosynek, K.C.C. Kharas, J.H. Lunsford, J. Catal. 132 (1991) 117.
[20] A.T. Ashcroft, A.K. Cheetham, J.S. Ford, M.L.H. Green, C.P. Grey, A.J. Murrell, P.D.F. Vernon, Nature 344 (1990) 319.
[21] F. van Looij, E.R. Stobbe, J.W. Geus, Catal. Lett. 50 (1998) 59.
[22] L.V. Mattos, E. Rodino, D.E. Resasco, F.B. Passos, F.B. Noronha, Fuel Process. Technol. 83 (2003) 147.